Lattice Boltzmann model for nonlinear convection-diffusion equations

Baochang Shi[*]
School of Mathematics and Statistics, Huazhong University of Science and Technology, Wuhan 430074, People's Republic of China

Zhaoli Guo[†]
State Key Laboratory of Coal Combustion, Huazhong University of Science and Technology,
Wuhan 430074, People's Republic of China

(Received 2 October 2007; published 6 January 2009)

A lattice Boltzmann model for convection-diffusion equation with nonlinear convection and isotropic-diffusion terms is proposed through selecting equilibrium distribution function properly. The model can be applied to the common real and complex-valued nonlinear evolutionary equations, such as the nonlinear Schrödinger equation, complex Ginzburg-Landau equation, Burgers-Fisher equation, nonlinear heat conduction equation, and sine-Gordon equation, by using a real and complex-valued distribution function and relaxation time. Detailed simulations of these equations are performed, and it is found that the numerical results agree well with the analytical solutions and the numerical solutions reported in previous studies.

DOI: 10.1103/PhysRevE.79.016701 PACS number(s): 02.70.−c, 02.60.Cb, 05.45.Yv

I. INTRODUCTION

The lattice Boltzmann method (LBM) is a new technique for simulating fluid flows and modeling complex physics in fluids [1–3]. Compared with the conventional computational fluid dynamics approach, the LBM is easy for programming, intrinsically parallel, and it is also easy to incorporate complicated boundary conditions such as those in porous media. In the past years, the lattice Bhatnagar-Gross-Krook (LBGK) model, the most popular LBM, has achieved great success in a variety of fields, ranging from simple laminar flows to thermal flows [4–6], compressible flows [7], porous media [8,9], blood flow [10], particle suspensions [11], multicomponent and multiphase systems [12,13], and so on. The LBM also shows potentials to simulate the nonlinear systems, such as reaction-diffusion equation [14–16], convection-diffusion equation (CDE) [5,17–21], Burgers equation [22], and wave equation [23]. However, they are commonly limited to isotropic diffusion. Recently, the LB models for advection and anisotropic dispersion equation have been proposed [24–26], among them the model by Ginzburg [26] is generic. In addition, Sman and Ernst studied the LBM for CDE deeply, and presented serval LB schemes (see Refs. [5,20] and references therein). The schemes on rectangular or irregular lattices developed by them are promising. It can be found that to recover the right macroscopic CDE, the appropriate assumptions are usually needed in the existing LB models.

Most of the existing LB models are used for real nonlinear systems. Since the mid 1990s, several types of quantum lattice gases and quantum LBM have been proposed based on quantum-computing ideas to model some real and complex mathematical-physical equations, such as the Dirac equation, Schrödinger equation, Gross-Pitaevskii equation, Burgers equation, KdV equation [27–36], etc. Although these models are not in the classical LBM framework and the multidimensional version of these models needs to be designed carefully [35], they bring us an interesting issue: how does the classical LBM work when used to model complex equations? Recently the LBM was applied to solve the one-dimensional nonlinear Schrödinger equation (NLSE) [37] using the idea of quantum lattice-gas model [30,31] to treat the reaction term. The simulation results show that the accuracy of the LB schemes is better than or at least comparable to that of the Crank-Nicolson finite difference scheme. In Ref. [38], motivated by the work in Ref. [37], LBM for n-dimensional (nD) CDE with a source term was directly applied to solve some nonlinear complex equations, including the NLS equation, coupled NLS equations, Klein-Gordon equation, and coupled Klein-Gordon-Schrödinger equations, by adopting a complex-valued distribution function and relaxation time. The simulations in Ref. [38] show that the LBM may be also an effective numerical solver for complex nonlinear systems.

However, the existing LB models are mainly for evolutionary equations with a linear convection or diffusion term. Although some recent LB models [24,26] can simulate the CDE with nonlinear convection or diffusion term, the additional assumptions on the convection and related terms are needed. In this paper, we present a LBGK model for a convection-diffusion equation with nonlinear convection and isotropic-diffusion terms through selecting equilibrium distribution function properly, and there is no additional assumption on the convection and diffusion terms. The model can be applied to the common real and complex-valued nonlinear evolutionary equations, such as NLSE, complex Ginzburg-Landau equation (CGLE), Burgers-Fisher equation (BFE), nonlinear heat conduction equation (NHCE), and sine-Gordon equation (SGE), by using real and complex-valued distribution function and relaxation time. Detailed simulations of these equations are performed, and numerical results agree well with the analytical and numerical solutions in the literature.

The rest of the paper is organized as follows. In Sec. II, the LBGK model for nonlinear convection-diffusion equation (NCDE) is presented and some of its special cases are

[*] sbchust@yahoo.com

[†] zlguo@hust.edu.cn

discussed, where the two schemes of the model for NCDE with nonlinear diffusion term are given. In Sec. III, the implemental version of the LBGK model for complex-valued NCDE is discussed. Numerical tests of the LBGK model are made in Sec. IV, and finally a brief summary is given in Sec. V.

II. LBGK MODEL

The nD NCDE with a source term considered in this paper can be written as

$$\partial_t \phi + \boldsymbol{\nabla} \cdot \mathbf{B}(\phi) = \boldsymbol{\nabla} \cdot [\alpha \boldsymbol{\nabla} D(\phi)] + F(\mathbf{x},t), \tag{1}$$

where $\boldsymbol{\nabla}$ is the gradient operator with respect to the spatial coordinate $\mathbf{x}$ in n dimensions. ϕ is a scalar function of position $\mathbf{x}$ and time t. $\alpha=\alpha(\mathbf{x},t)$ is the diffusion coefficient. $\mathbf{B}$ and D are the known differential functions of ϕ and $F(\mathbf{x},t)$ is the source term.

There is relatively less work on LB models for solving Eq. (1). In Ref. [26], two LB models for generic advection and anisotropic-dispersion equation were proposed, which can be used to solve Eq. (1). However, to recover the macroscopic equation, the additional assumptions (Secs. 4.3.2 and 5.2 in Ref. [26]) on the convection and related terms are needed. These assumptions may not be satisfied. For example, they are not satisfied for the case $\mathbf{B}(\phi)=\phi^2\mathbf{I}$ and for example 4.3 below.

Our LBGK model is based on the DnQb lattice [2] with b velocity directions in nD space, and we use one of the LBGK schemes in Ref. [21] for treating the source term. The evolution equation of the distribution function in the model reads

$$f_j(\mathbf{x}+\mathbf{c}_j\Delta t, t+\Delta t) = f_j(\mathbf{x},t) - \frac{1}{\tau}[f_j(\mathbf{x},t) - f_j^{\text{eq}}(\mathbf{x},t)] + \Delta t F_j(\mathbf{x},t) + \frac{\theta \Delta t^2}{2}\partial_t F_j(\mathbf{x},t),$$

$$j=0,\ldots,b-1, \tag{2}$$

where $\{\mathbf{c}_j, j=0,\ldots,b-1\}$ is the set of discrete velocity directions, Δt is the time step, τ is the dimensionless relaxation time, $f_j^{\text{eq}}(\mathbf{x},t)$ is the equilibrium distribution function, and $F_j(\mathbf{x},t)$ the distribution function for the source term.

Note that θ in Eq. (2) is a real parameter, corresponding to the standard LBGK model for $\theta=0$ and a scheme in Ref. [21] for $\theta=1$, respectively. When $\theta=1$, the additional term in the recovered macroscopic equation can be removed (see below). Other LBGK schemes in Ref. [21] can also be used. For simplicity, we only use the simpler one.

To solve Eq. (1) using the LB equation (2) without additional assumptions, we must give appropriate $f_j^{\text{eq}}(\mathbf{x},t)$ and $F_j(\mathbf{x},t)$. As pointed in the general parallel analysis of LBM for convection diffusion and fluid flow in Ref. [5], reasonable constraints of moments of the equilibrium distribution $f_j^{\text{eq}}(\mathbf{x},t)$ must be satisfied. Keeping this in mind and following the common LBGK model, we take the equilibrium distribution function as

$$f_j^{\text{eq}} = \omega_j\left[\phi + \frac{\mathbf{c}_j\cdot\mathbf{B}}{c_s^2} + \frac{(\mathbf{C}-c_s^2\phi\mathbf{I}):(\mathbf{c}_j\mathbf{c}_j - c_s^2\mathbf{I})}{2c_s^4}\right], \tag{3}$$

where $\mathbf{I}$ is the unit tensor, $\mathbf{C}(\phi)=\mathbf{C}_0(\phi)+c_s^2 D(\phi)\mathbf{I}$ is the second order moment of f_j^{eq}, and $\mathbf{C}_0(\phi)$ is a tensor function of ϕ, which will be determined later. ω_j are weights and c_s, the so called sound speed in the LBM, is related to the particle speed c and ω_j by $\Sigma_j \omega_j \mathbf{c}_j\mathbf{c}_j = c_s^2\mathbf{I}$, and they all depend on the lattice model used, where $c=\Delta x/\Delta t$ and Δx is the lattice spacing. Note that the second term in $\mathbf{C}(\phi)$ is similar to that in the Cahn-Hilliard model [17] with $D(\phi)$ equal to chemical potential, while $\mathbf{C}_0(\phi)$ is a new one which is used to remove some additional terms in the recovered macroscopic equation.

The parameters are given as follows: for the D1Q3 model, $\{\mathbf{c}_0,\mathbf{c}_1,\mathbf{c}_2\}=\{0,c,-c\}$, $\omega_0=2/3$, $\omega_1=\omega_2=1/6$; for the D2Q9 one, $\{\mathbf{c}_j, j=0,\ldots,8\}=\{(0,0),(\pm c,0),(0,\pm c),(\pm c,\pm c)\}$, $\omega_0=4/9$, $\omega_{1\sim 4}=1/9$, $\omega_{5\sim 8}=1/36$, then $c_s^2=c^2/3$ for both of them. ϕ is determined by $\phi=\Sigma_j f_j$, and f_j and f_j^{eq} satisfy

$$\sum_j f_j = \sum_j f_j^{\text{eq}} = \phi,$$

$$\sum_j \mathbf{c}_j f_j^{\text{eq}} = \mathbf{B}(\phi), \sum_j \mathbf{c}_j\mathbf{c}_j f_j^{\text{eq}} = \mathbf{C}(\phi). \tag{4}$$

The corresponding source term F_j is taken as

$$F_j = \omega_j F\left[1 + \lambda\frac{\mathbf{c}_j\cdot\mathbf{B}'(\phi)}{c_s^2}\right] \tag{5}$$

such that $\Sigma_j F_j = F$, $\Sigma_j \mathbf{c}_j F_j = \lambda F \mathbf{B}'(\phi)$, where $\mathbf{B}'=\frac{d\mathbf{B}}{d\phi}$, and λ is another parameter to be determined.

To derive the macroscopic equation (1), the Chapman-Enskog expansion in time and space is applied:

$$f_j = f_j^{\text{eq}} + \epsilon f_j^{(1)} + \epsilon^2 f_j^{(2)},$$

$$F = \epsilon F^{(1)}, \quad \partial_t = \epsilon\partial_{t_1} + \epsilon^2\partial_{t_2}, \quad \boldsymbol{\nabla} = \epsilon\boldsymbol{\nabla}_1, \tag{6}$$

where ϵ is a small expansion parameter. Using Eq. (6), the first formula in Eq. (4), and Eq. (5), we have

$$\sum_j f_j^{(k)} = 0 (k \geqslant 1),$$

$$\sum_j F_j^{(1)} = F^{(1)}, \quad \sum_j \mathbf{c}_j F_j^{(1)} = \lambda F^{(1)}\mathbf{B}'(\phi), \tag{7}$$

where $F_j^{(1)} = \omega_j F^{(1)}[1+\lambda\frac{\mathbf{c}_j\cdot\mathbf{B}'(\phi)}{c_s^2}]$.

By applying Taylor expansion to Eq. (2), we get

$$D_j f_j + \frac{\Delta t}{2}D_j^2 f_j + \cdots = -\frac{1}{\tau\Delta t}(f_j - f_j^{\text{eq}}) + F_j + \frac{\theta\Delta t}{2}\partial_t F_j(\mathbf{x},t), \tag{8}$$

where $D_j=\partial_t + \mathbf{c}_j\cdot\boldsymbol{\nabla}$. Denote $D_{1j}=\partial_{t_1}+\mathbf{c}_j\cdot\boldsymbol{\nabla}_1$. Substituting Eq. (6) into Eq. (8) and treating the terms in order of ϵ and ϵ^2 separately gives

$$D_{1j} f_j^{\text{eq}} = -\frac{1}{\tau\Delta t} f_j^{(1)} + F_j^{(1)}, \tag{9a}$$

$$\partial_{t_2} f_j^{\text{eq}} + D_{1j} f_j^{(1)} + \frac{\Delta t}{2} D_{1j}^2 f_j^{\text{eq}} = -\frac{1}{\tau \Delta t} f_j^{(2)} + \frac{\theta \Delta t}{2} \partial_{t_1} F_j^{(1)}. \tag{9b}$$

Applying Eq. (9a) to the left side of Eq. (9b) and collecting the terms related to $\frac{\Delta t}{2}\partial_{t_1} F_j^{(1)}$ on the both sides, we can rewrite Eq. (9b) as

$$\partial_{t_2} f_j^{\text{eq}} + D_{1j}\left[\left(1 - \frac{1}{2\tau}\right) f_j^{(1)}\right] + \frac{\Delta t}{2}\mathbf{c}_j \cdot \nabla_1 F_j^{(1)} = -\frac{1}{\tau \Delta t} f_j^{(2)} + \frac{(\theta - 1)\Delta t}{2}\partial_{t_1} F_j^{(1)}. \tag{10}$$

Summing Eqs. (9a) and (10) over j and using Eqs. (4) and (7), we obtain

$$\partial_{t_1}\phi + \nabla_1 \cdot \mathbf{B}(\phi) = F^{(1)}, \tag{11}$$

$$\partial_{t_2}\phi + \nabla_1 \cdot \left[\left(1 - \frac{1}{2\tau}\right)\sum_j \mathbf{c}_j f_j^{(1)}\right] + \frac{\Delta t}{2}\nabla_1 \cdot [\lambda F^{(1)}\mathbf{B}'(\phi)] = \frac{(\theta - 1)\Delta t}{2}\partial_{t_1} F^{(1)}. \tag{12}$$

Using Eqs. (9a), (4), and (7), we have

$$\begin{aligned}\sum_j \mathbf{c}_j f_j^{(1)} &= -\tau \Delta t \sum_j \mathbf{c}_j (D_{1j} f_j^{\text{eq}} - F_j^{(1)}) \\ &= -\tau \Delta t[\partial_{t_1}\mathbf{B}(\phi) + \nabla_1 \cdot \mathbf{C}(\phi) - \lambda F^{(1)}\mathbf{B}'(\phi)] \\ &= -\tau \Delta t[\mathbf{B}'(\phi)\partial_{t_1}\phi + \mathbf{C}_0'(\phi) \cdot \nabla_1 \phi + c_s^2 \nabla_1 D(\phi) \\ &\quad - \lambda F^{(1)}\mathbf{B}'(\phi)].\end{aligned} \tag{13}$$

If we take $\mathbf{C}_0'(\phi) = \mathbf{B}'(\phi)\mathbf{B}'(\phi)$, then it follows from Eqs. (13) and (11) that

$$\begin{aligned}\sum_j \mathbf{c}_j f_j^{(1)} &= -\tau \Delta t \mathbf{B}'(\phi)[\partial_{t_1}\phi + \nabla_1 \cdot \mathbf{B}(\phi) - F^{(1)}] \\ &\quad - \tau \Delta t[(1 - \lambda)F^{(1)}\mathbf{B}'(\phi) + c_s^2 \nabla_1 D(\phi)] \\ &= -\tau \Delta t[(1 - \lambda)F^{(1)}\mathbf{B}'(\phi) + c_s^2 \nabla_1 D(\phi)].\end{aligned} \tag{14}$$

So, substituting Eq. (14) into Eq. (12), we obtain

$$\begin{aligned}\partial_{t_2}\phi &= \nabla_1 \cdot \left\{\left[c_s^2\left(\tau - \frac{1}{2}\right)\Delta t\right]\nabla_1 D(\phi)\right\} \\ &\quad - \Delta t \nabla_1 \cdot \left\{\left[\tau\lambda - \left(\tau - \frac{1}{2}\right)\right] F^{(1)}\mathbf{B}'(\phi)\right\} \\ &\quad + \frac{(\theta - 1)\Delta t}{2}\partial_{t_1} F^{(1)}.\end{aligned} \tag{15}$$

Combining Eqs. (15) and (11) and taking

$$\alpha = c_s^2\left(\tau - \frac{1}{2}\right)\Delta t, \tag{16}$$

we have

$$\begin{aligned}\partial_t \phi + \nabla \cdot \mathbf{B}(\phi) &= \nabla \cdot [\alpha \nabla D(\phi)] \\ &\quad + F - \Delta t \nabla \cdot \left\{\left[\tau\lambda - \left(\tau - \frac{1}{2}\right)\right] F\mathbf{B}'(\phi)\right\} \\ &\quad + \frac{(\theta - 1)\epsilon \Delta t}{2}\partial_{t_1} F.\end{aligned} \tag{17}$$

Now, taking $\lambda = \frac{(\tau - 1/2)}{\tau}$ and $\theta = 1$ to remove the two additional terms in Eq. (17), the NCDE (1) is exactly recovered to order $O(\epsilon^2)$.

Remark 1. It can be found from the analysis above that for the standard LBGK ($\theta = 0$) or for that $\theta \neq 1$, there must be an additional term $(\theta - 1)(\Delta t/2)\epsilon \partial_{t_1} F$ in Eq. (17). This term can also be deleted by using a redefinition for the convective flux as suggested in literature [39]. However, the redefinition scheme cannot be used directly for the NCDE (1) since it is implicit when F is a nonlinear function of ϕ, while the scheme here ($\theta = 1$) can since the explicit difference scheme can be used for computing $\partial_t F_j(\mathbf{x}, t)$ [21]. It should be noted that in the standard LBGK model there is no need for the redefinition for CDE coupled with weakly compressible fluid flow, and the detailed analysis can be found in Ref. [5].

Remark 2. It should be noted that when $\mathbf{B} = \mathbf{0}$, Eq. (1) becomes the nonlinear diffusion equation with a source term. In this case, $\mathbf{C}(\phi) = c_s^2 D(\phi)\mathbf{I}$ and the equilibrium and source distribution functions are of simple forms

$$\begin{aligned}f_j^{\text{eq}} &= \omega_j\left[\phi + \frac{\{[D(\phi) - \phi]\mathbf{I}\}:(\mathbf{c}_j\mathbf{c}_j - c_s^2\mathbf{I})}{2c_s^2}\right] \\ &= \omega_j\left[\phi + \frac{[D(\phi) - \phi](\mathbf{c}_j^2 - c_s^2 d)}{2c_s^2}\right],\end{aligned}$$

$$F_j = \omega_j F, \tag{18}$$

where d is the dimensions. Now the DdQ($2d+1$) lattice model can also be used, which leads to a simpler LBGK model. For this model f_j^{eq} is not of the form of Eq. (18), and from Eq. (4) it can be easily obtained that $f_0^{\text{eq}} = \phi - 2d\omega_1 D(\phi)$, $f_j^{\text{eq}} = \omega_1 D(\phi), j \neq 0$, where $\omega_0 + 2d\omega_1 = 1$. Furthermore, for the case $D(\phi) = \phi$, f_j^{eq} in Eq. (18) reduces to the simplest form $f_j^{\text{eq}} = \omega_j \phi$, the same as F_j.

Remark 3. For the case $\mathbf{B} \neq \mathbf{0}$, we can take $\mathbf{C}_0(\phi)$ such that $[\mathbf{C}_0(\phi)]_{\alpha\beta} = \int \mathbf{B}'_\alpha(\phi)\mathbf{B}'_\beta(\phi)d\phi$. When $\mathbf{B}$ and D are known, the different CDEs can be obtained.

Remark 4. Rewrite Eq. (1) as

$$\partial_t \phi + \nabla \cdot \mathbf{B}(\phi) = \nabla \cdot (\tilde{\alpha} \nabla \phi) + F(\mathbf{x}, t), \tag{19}$$

where $\tilde{\alpha} = \alpha D'(\phi)$.

Using above LBGK model to solve Eq. (19), we have

$$f_j^{\text{eq}} = \omega_j\left[\phi + \frac{\mathbf{c}_j \cdot \mathbf{B}}{c_s^2} + \frac{\mathbf{C}_0:(\mathbf{c}_j\mathbf{c}_j - c_s^2\mathbf{I})}{2c_s^4}\right] \tag{20}$$

and

$$\tilde{\alpha} = c_s^2\left(\tau - \frac{1}{2}\right)\Delta t. \quad (21)$$

This leads to another LBGK scheme for Eq. (1). So, if $D(\phi) \neq \phi$, two LBGK schemes for Eq. (1) can be derived. Scheme 1: Eqs. (2) and (3) with Eq. (16); scheme 2: Eqs. (2) and (20) with Eq. (21).

III. LBGK MODEL FOR COMPLEX NCDE

Almost all of the existing LBGK models are designed for real evolutionary equations. However, from the Chapman-Enskog analysis in above section, we can see that the functions in NCDE and related distribution function can be both real and complex without affecting the results.

Following the idea of solving the complex evolutionary equations by LBGK model in Ref. [38], we can define the complex variables as

$$f_j = g_j + ih_j, \quad f_j^{\mathrm{eq}} = g_j^{\mathrm{eq}} + ih_j^{\mathrm{eq}},$$

$$F_j = G_j + iH_j, \quad w = \frac{1}{\tau} = w_1 + iw_2, \quad (22)$$

where $i^2=-1$. Then we can rewrite Eq. (2) as

$$\begin{aligned} g_j(\mathbf{x}+\mathbf{c}_j\Delta t, t+\Delta t) = {} & g_j(\mathbf{x},t) - w_1[g_j(\mathbf{x},t) - g_j^{\mathrm{eq}}(\mathbf{x},t)] \\ & + w_2[h_j(\mathbf{x},t) - h_j^{\mathrm{eq}}(\mathbf{x},t)] + \Delta t G_j(\mathbf{x},t) \\ & + \frac{\theta\Delta t^2}{2}\partial_t G_j(\mathbf{x},t), \end{aligned}$$

$$\begin{aligned} h_j(\mathbf{x}+\mathbf{c}_j\Delta t, t+\Delta t) = {} & h_j(\mathbf{x},t) - w_2[g_j(\mathbf{x},t) - g_j^{\mathrm{eq}}(\mathbf{x},t)] \\ & - w_1[h_j(\mathbf{x},t) - h_j^{\mathrm{eq}}(\mathbf{x},t)] + \Delta t H_j(\mathbf{x},t) \\ & + \frac{\theta\Delta t^2}{2}\partial_t H_j(\mathbf{x},t), \end{aligned}$$

$$j = 0, \ldots, b-1. \quad (23)$$

Equation (23) is the implemental version of the LBGK model (2) for complex NCDE. It should be noted that Eq. (23) reflects the coupling effect of the real part and the imaginary one of the unknown function in complex NCDE through the complex-valued relaxation time in a natural way. In fact, let $\tau=\tau_1+i\tau_2, \alpha=\alpha_1+i\alpha_2$, then from Eqs. (16) and (22) we have

$$\tau_1 = \frac{\alpha_1}{c_s^2\Delta t} + \frac{1}{2}, \quad \tau_2 = \frac{\alpha_2}{c_s^2\Delta t}, \quad w_1 = \frac{\tau_1}{\tau_1^2+\tau_2^2}, \quad w_2 = -\frac{\tau_2}{\tau_1^2+\tau_2^2}. \quad (24)$$

From Eq. (24), we can see that if α is a complex variable, that is, $\alpha_2 \neq 0$, then $w_2 \neq 0$. At this time, Eq. (23) is coupled and $\tau_1 > \frac{1}{2}$ is not necessary. Otherwise, $\tau_2 = w_2 = 0$, $w_1 = \frac{1}{\tau_1}$, and Eq. (23) is decoupled.

IV. SIMULATION RESULTS

To test the LBGK model proposed above, numerical simulations of some CDEs are performed. In all simulations, if not specified, we use the nonequilibrium extrapolation scheme proposed by Guo *et al.* [40] to treat the boundary condition except for the periodic one, and the initial and boundary conditions of the test problems with analytical solutions are determined by their analytical solutions. The D1Q3 and D2Q9 LBGK models are used to simulate the 1D and 2D test problems, respectively, and the explicit difference scheme $\partial_t F_j(\mathbf{x},t) = [F_j(\mathbf{x},t) - F_j(\mathbf{x},t-\Delta t)]/\Delta t$, is used for computing $\partial_t F_j(\mathbf{x},t)$. The following global relative error is used to measure the accuracy:

$$E = \frac{\sum_j |\phi(\mathbf{x}_j,t) - \phi^*(\mathbf{x}_j,t)|}{\sum_j |\phi^*(\mathbf{x}_j,t)|}, \quad (25)$$

where ϕ and ϕ^* are the numerical solution and analytical one, respectively, and the summation is taken over all grid points.

For comparison we use two LBGK models to simulate the problems with analytical solutions. One is the model using standard LBGK evolution equation ($\theta=0$) and the other is the proposed model ($\theta=1$), which are denoted by methods 1 and 2, respectively. Method 2 is used to simulate the rest of the problems.

Since the accuracy tests of some complex nonlinear equations have been made in Refs. [37,38], here we only test the double soliton collision of 1D NLSE [41] and the X and target waves of 2D cubic CGLE [42]. The other test problems are all real equations.

Example 4.1. The double soliton collision of 1D NLSE [41]

$$iu_t + u_{xx} + 2|u|^2 u = 0, \quad (26)$$

with the initial condition

$$u(x,0) = \sum_{j=1}^{2} \exp\left(\frac{1}{2}ic_j(x-x_j)\right)\mathrm{sech}(x-x_j), \quad (27)$$

where c_1, x_1, c_2, x_2 are parameters.

In simulations, we set $c_1=4$, $x_1=-10$, $c_2=-4$, $x_2=10$ as in Ref. [41]. The simulation is conducted with periodic boundary condition in $[-25,25]$ with $\Delta x=0.01$, $\Delta t=0.0001$. The results are shown in Fig. 1. It can be found that the LBGK results are is in excellent agreement with those in Ref. [41].

Example 4.2. The X and target waves of 2D cubic CGLE [42]

$$u_t = \mu(\mathbf{x})u + (1+i\alpha)\nabla^2 u - (1+i\beta)|u|^2 u, \quad (28)$$

with periodic boundary condition and random initial condition, where $\mu(x,y) = 1 - \frac{1}{2}\Omega^2(x^2+y^2)$, Ω is the Einstein frequency.

It has been found that when $\Omega=0$, 0.01 and 0.02, the spiral, X and target waves are formed, respectively, for CGLE (28) with $\alpha=3.5$ and $\beta=-0.34$ [42]. Here we use the LBGK model to reproduce the X and target waves.

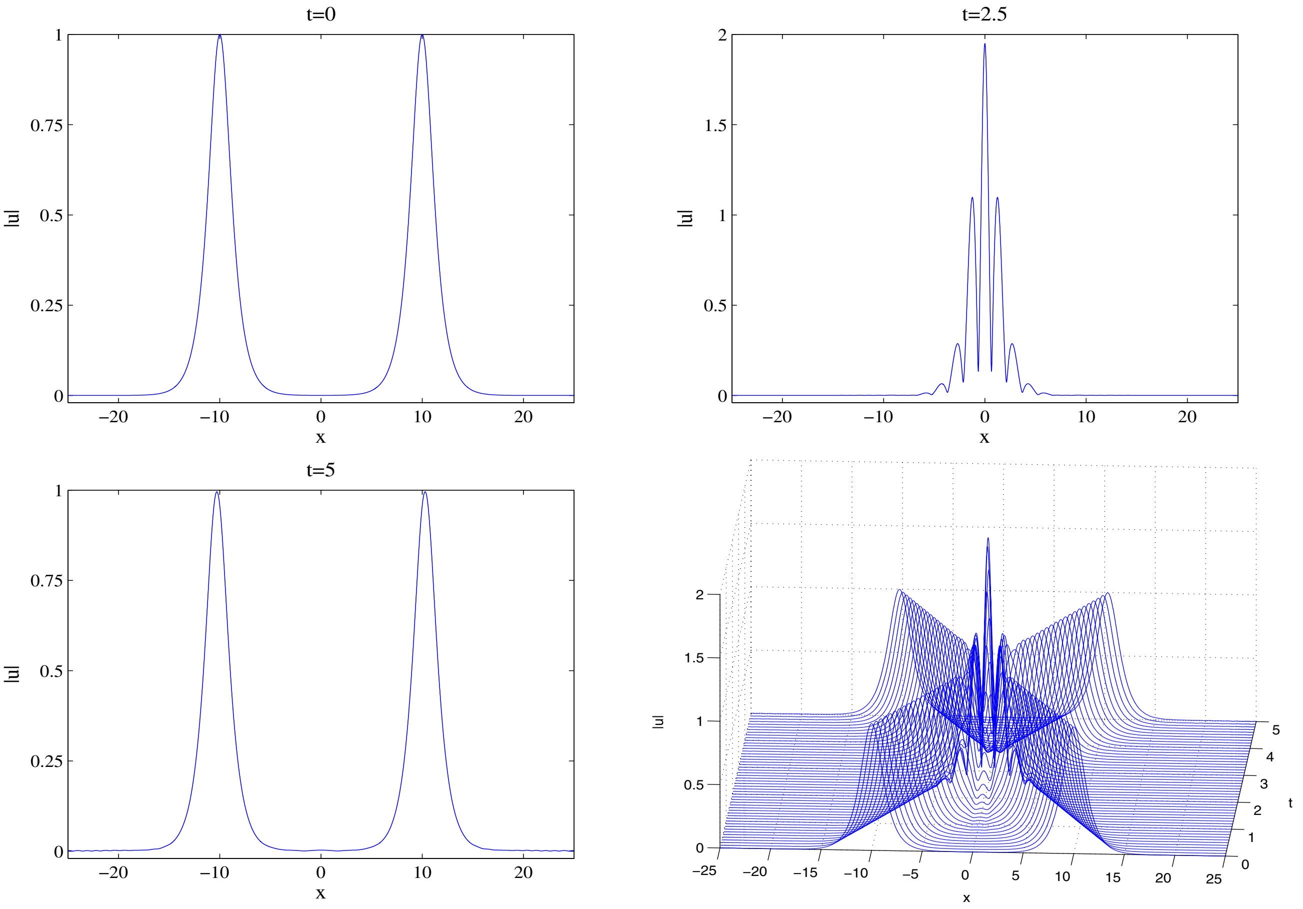

FIG. 1. (Color online) Collision of two solitons of 1D NLSE at different times.

In the simulation the initial condition is taken as $\mathrm{Re}[u(x,y,0)]=10^{-6}\mathrm{rand}(\cdots)$, $\mathrm{Im}[u(x,y,0)]=10^{-6}\mathrm{rand}(\cdots)$, where $\mathrm{rand}(\cdots)$ is a random function in C++. The simulation results are performed on $[-100,100]\times[-100,100]$ with $\Delta x=1.0$ and $\Delta t=0.01$. The results are shown in Figs. 2 and 3. It is seen that the numerical results in Figs. 2 and 3 agree well with those in Ref. [42]. It should be noted that we have not reproduced the spiral wave for $\Omega=0$ by using the LBGK model with the initial condition above.

Example 4.3. The BFE in two dimensions [43]

$$u_t + au^{\delta}u_x - b(u_{xx}+u_{yy}) - ku(1-u^{\delta}) = 0, \quad \delta > 1 \quad (29)$$

with the analytical solution

$$u(x,y,t) = \left\{\frac{1}{2} + \frac{1}{2}\tanh[A(x+y-\omega t)]\right\}^{1/\delta}, \quad (30)$$

where $A=-\frac{a\delta}{4b(\delta+1)}$, $\omega=\frac{a^2+2bk(\delta+1)^2}{a(\delta+1)}$, a, b, k, and δ are real constants.

For Eq. (29), $\mathbf{B}(u)=(\frac{a}{\delta+1},0)^T u^{\delta+1}$, so we can take $\mathbf{C}_0$ such that $[\mathbf{C}_0(u)]_{11}=\frac{a^2}{2\delta+1}u^{2\delta+1}$, $[\mathbf{C}_0(u)]_{\alpha\beta}=0$, $(\alpha,\beta)\neq(1,1)$. The simulations are performed on $[-1,2]\times[-1,2]$ for different parameters by using methods 1 and 2, respectively, for comparison. The effects of the parameters a, b and c on the methods are mainly studied since those of the parameters δ and k are relatively small. Here we set $\delta=1.5$ and $k=1$. The global relative errors at $t=0.5$ and $t=1$ on a 300×300 grid for different parameters are listed in Table I. From the table it can be found that in most of the cases the errors at $t=1$ are smaller than those at $t=0.5$, and when the parameters other than the time step are fixed, the errors decrease as the time step decreases or the particle speed c increases. It can also be found that method 1 is a little more accurate than method 2, which shows that for the test case here the modification of evolution equation does not bring the expected effect. The numerical solutions by method 2 together with the analytical ones at $x=0.5$ for $a=6$, $b=0.05$, $c=10$ and different time steps are plotted in Fig. 4.

To test the accuracy of the two methods, the global relative errors and global maximum errors are plotted in Fig. 5 at time $t=0.5$ and $t=1$ with different resolutions, range from $\Delta x=1/20$ to 1/160 and $c=5$ to 40, for $a=4.0$ and $b=0.1$. For method 1 the orders of global relative errors are found to be 1.9123, 1,9525, 1.9653 for $t=0.5$, and 2.0203, 1.9809, 1.9750 for $t=1$, respectively, while for method 2 the orders are 1.9364, 1.9539, 1.9672 for $t=0.5$, and 2.0307, 1.9826, 1.9765 for $t=1$, respectively. It is shown that both of the two methods for above BFE are of the second order of accuracy. From Table I, Figs. 4 and 5 it can be seen that the LBM works well for the BFE.

Example 4.4. The generalized NHCE in two dimensions [43]

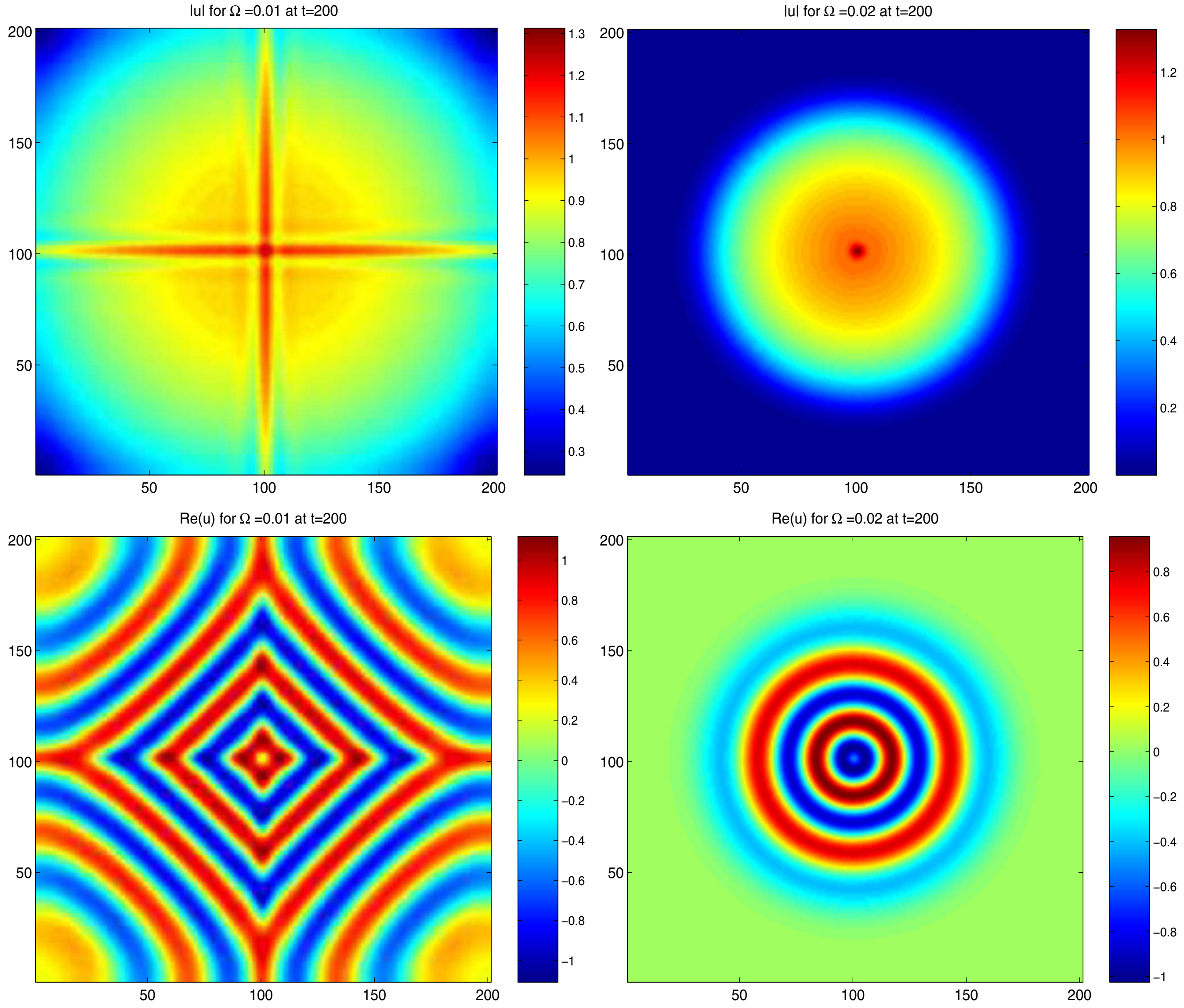

FIG. 2. (Color online) *X* wave (left) and target wave (right).

$$u_t - \alpha(u^\delta)_{xx} - \alpha(u^\delta)_{yy} - u + u^\delta = 0, \quad \delta > 1 \tag{31}$$

with the analytical solution

$$u(x,y,t) = \left\{ \frac{1}{2} - \frac{1}{2}\tanh\left[\frac{\delta - 1}{2\delta\sqrt{2\alpha}}(x + y - \sqrt{2\alpha}t) \right] \right\}^{-1/(\delta-1)}, \tag{32}$$

where α and δ are real constants.

For Eq. (31), $\mathbf{B}=0$, $D(u)=u^\delta$, and $\mathbf{C}=c_s^2 u^\delta \mathbf{I}$, thus following Eq. (18), Eq. (3) is simplified as for scheme 1

$$f_j^{\rm eq} = \omega_j u \left[1 + \frac{(u^{\delta-1} - 1)(\mathbf{c}_j^2 - 2c_s^2)}{2c_s^2} \right], \quad F_j = \omega_j(u - u^\delta) \tag{33}$$

with $c_s^2(\tau - \frac{1}{2})\Delta t = \alpha$, while for scheme 2

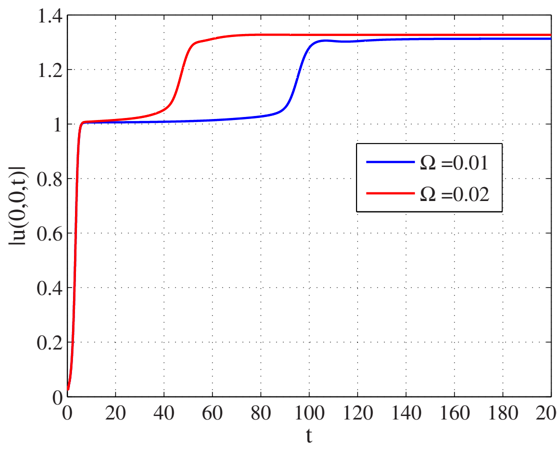

FIG. 3. (Color online) The evolution of the amplitude $|u(0,0,t)|$ at the center of the simulated system for $\Omega=0.01$ (bottom) and 0.02 (top), corresponding to the *X* and target patterns, respectively.

TABLE I. Global relative errors for $\delta=1.5$ and $k=1.0$ at $t=0.5$ and $t=1$ [(1) $t=0.5$, (2) $t=1$; $M1$: method 1, $M2$: method 2].

			$c=10$			$c=20$		
b			$a=2$	$a=4$	$a=6$	$a=2$	$a=4$	$a=6$
$b=0.05$	(1)	$M1$	2.5198×10^{-4}	1.0133×10^{-3}	1.3969×10^{-3}	6.5987×10^{-5}	2.5215×10^{-4}	3.3463×10^{-4}
		$M2$	2.8787×10^{-4}	1.0360×10^{-3}	1.4093×10^{-3}	8.6553×10^{-5}	2.6398×10^{-4}	3.4109×10^{-4}
	(2)	$M1$	3.6216×10^{-4}	7.2002×10^{-4}	6.8001×10^{-4}	8.5873×10^{-5}	1.7170×10^{-4}	1.5980×10^{-4}
		$M2$	4.0733×10^{-4}	7.3538×10^{-4}	6.8605×10^{-4}	1.0916×10^{-4}	1.7942×10^{-4}	1.6276×10^{-4}
$b=0.10$	(1)	$M1$	3.7744×10^{-4}	1.4628×10^{-3}	2.3889×10^{-3}	9.2339×10^{-5}	3.7426×10^{-4}	5.8634×10^{-4}
		$M2$	3.4131×10^{-4}	1.5000×10^{-3}	2.4110×10^{-3}	7.6085×10^{-5}	3.9306×10^{-4}	5.9743×10^{-4}
	(2)	$M1$	2.8280×10^{-4}	1.0924×10^{-3}	1.1155×10^{-3}	6.6644×10^{-5}	2.6959×10^{-4}	2.7083×10^{-4}
		$M2$	3.1880×10^{-4}	1.1176×10^{-3}	1.1256×10^{-3}	8.9309×10^{-5}	2.8206×10^{-4}	2.7573×10^{-4}
$b=0.50$	(1)	$M1$	6.9318×10^{-4}	1.9134×10^{-3}	2.8168×10^{-3}	1.9734×10^{-4}	4.7911×10^{-4}	6.5722×10^{-4}
		$M2$	6.6438×10^{-4}	1.8769×10^{-3}	2.8098×10^{-3}	1.8236×10^{-4}	4.6219×10^{-4}	6.6020×10^{-4}
	(2)	$M1$	4.3357×10^{-4}	1.1099×10^{-3}	1.5833×10^{-3}	1.1457×10^{-4}	2.6628×10^{-4}	3.4373×10^{-4}
		$M2$	4.2175×10^{-4}	1.1103×10^{-3}	1.5876×10^{-3}	1.0722×10^{-4}	2.6690×10^{-4}	3.4586×10^{-4}
$b=1.00$	(1)	$M1$	5.8622×10^{-4}	1.6295×10^{-3}	3.1786×10^{-3}	1.6094×10^{-4}	4.1877×10^{-4}	7.4067×10^{-4}
		$M2$	5.7306×10^{-4}	1.6085×10^{-3}	3.1543×10^{-3}	1.5438×10^{-4}	4.0948×10^{-4}	7.3237×10^{-4}
	(2)	$M1$	3.0302×10^{-4}	9.4370×10^{-4}	1.7704×10^{-3}	8.8190×10^{-5}	2.3428×10^{-4}	4.2510×10^{-4}
		$M2$	2.8400×10^{-4}	9.3798×10^{-4}	1.7736×10^{-3}	7.7845×10^{-5}	2.3261×10^{-4}	4.2834×10^{-4}

$$f_j^{\mathrm{eq}}=\omega_j u, \quad F_j=\omega_j(u-u^{\delta}) \tag{34}$$

with $c_s^2(\tau-\frac{1}{2})\Delta t=\alpha\delta u^{\delta-1}$.

The simulations are performed on $[0,1]\times[0,1]$ for different parameters by using methods 1 and 2 for comparison, and for each method, schemes 1 and 2 are used, respectively. The global relative errors on a 100×100 grid at $t=1$ for different parameters are listed in Table II. Similarly, from the table it can be found that in most of the cases when the parameters other than the time step are fixed, the errors decrease obviously as the time step decreases or the particle speed c increases. We find that method 2 is more accurate than method 1, but the difference is small. However, it is worthy noticing that for the case of $\alpha=0.01$ the errors do not decrease but increase as the time step decreases or c increases.

To test the accuracy of the two methods, the global relative errors and global maximum errors are plotted in Fig. 6 at time $t=1$ in different resolutions, from $\Delta x=1/10$ to $1/640$ and $c=1$ to 64, for $\delta=1.2$ and $\alpha=0.01$. It is found that both of the two methods for the NHCE (31) are of second-order accuracy on the finer grids. The order of global relative errors by method 1 increases from 1.5828 to 1.9744 for scheme 1 and from 1.8163 to 1.9902 for scheme 2, respec-

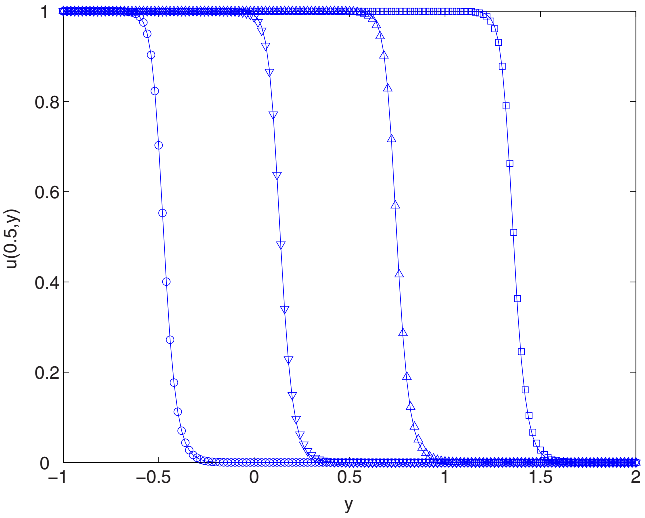

FIG. 4. (Color online) Comparison of analytical solutions with numerical solutions at $x=0.5$ for different time steps: $t=0$, 0.25, 0.5, and 0.75. Solid lines: analytical solutions; symbols: numerical ones.

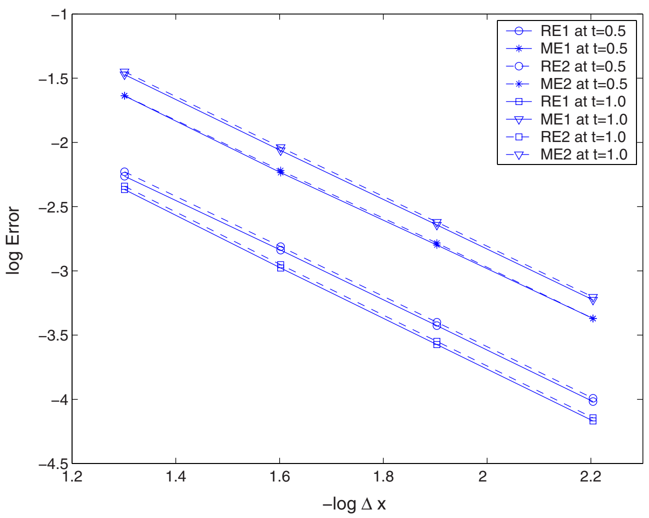

FIG. 5. (Color online) Accuracy test at $t=0.5$ and 1 for $\delta=1.5$, $a=4.0$, $b=0.1$, and $k=1$. RE and ME: global relative and maximum errors; 1 and 2: the results obtained by methods 1 and 2.

TABLE II. Comparison of global relative errors at $t=1$. [(1) $\delta=1.2$, (2) $\delta=1.5$; $M1$: method 1, $M2$: method 2. 'Blanks' mean that the scheme is divergent.]

			Scheme 1			Scheme 2		
α			$c=10$	$c=20$	$c=100$	$c=10$	$c=20$	$c=100$
$\alpha=0.01$	(1)	$M1$	4.6981×10^{-5}			7.7092×10^{-5}	4.1524×10^{-5}	9.7853×10^{-5}
		$M2$	3.8456×10^{-5}			4.0878×10^{-5}	4.1133×10^{-5}	1.0130×10^{-4}
	(2)	$M1$	1.8458×10^{-5}			2.8091×10^{-5}	1.3148×10^{-5}	3.1951×10^{-5}
		$M2$	1.2584×10^{-5}			1.5588×10^{-5}	1.2306×10^{-5}	3.3037×10^{-5}
$\alpha=0.05$	(1)	$M1$	6.2575×10^{-5}	3.2158×10^{-5}		1.6827×10^{-4}	7.8142×10^{-5}	1.3220×10^{-5}
		$M2$	7.2409×10^{-5}	1.6379×10^{-5}		1.8296×10^{-4}	6.3562×10^{-5}	1.6272×10^{-5}
	(2)	$M1$	3.8496×10^{-5}	1.4609×10^{-5}		1.3635×10^{-4}	3.6084×10^{-5}	5.7715×10^{-6}
		$M2$	4.8209×10^{-5}	8.4623×10^{-6}		1.4843×10^{-4}	3.6193×10^{-5}	7.1173×10^{-6}
$\alpha=0.10$	(1)	$M1$	1.1843×10^{-4}	3.8315×10^{-5}	8.7176×10^{-6}	3.1122×10^{-4}	8.9968×10^{-5}	9.2293×10^{-6}
		$M2$	1.3169×10^{-4}	3.5383×10^{-5}	1.0990×10^{-5}	3.2520×10^{-4}	9.0404×10^{-5}	6.9615×10^{-6}
	(2)	$M1$	9.2449×10^{-5}	2.1623×10^{-5}		3.0190×10^{-4}	6.9183×10^{-5}	6.6177×10^{-6}
		$M2$	1.0211×10^{-4}	2.2794×10^{-5}		3.1217×10^{-4}	7.2337×10^{-5}	5.2568×10^{-6}
$\alpha=1.00$	(1)	$M1$	3.1222×10^{-4}	1.0050×10^{-4}	1.9763×10^{-5}	1.0016×10^{-3}	3.6451×10^{-4}	4.5857×10^{-5}
		$M2$	3.0901×10^{-4}	9.8807×10^{-5}	1.9437×10^{-5}	9.9961×10^{-4}	3.6319×10^{-4}	4.5538×10^{-5}
	(2)	$M1$	1.8651×10^{-4}	6.3352×10^{-5}	1.3865×10^{-5}	8.1274×10^{-4}	2.8591×10^{-4}	3.4819×10^{-5}
		$M2$	1.8478×10^{-4}	6.2805×10^{-5}	1.3628×10^{-5}	8.1138×10^{-4}	2.8500×10^{-4}	3.4583×10^{-5}

tively, as the grid resolution increases, while the order of global relative errors by method 2 increases from 1.5272 to 1.9694 for scheme 1 and from 1.8077 to 1.9848 for scheme 2, respectively. Clearly the accuracy of scheme 2 is generally lower than that of scheme 1, but the stability of the former is much better than that of the latter. From Table II and Fig. 6 it can be seen that the LBM also works well for NHCE. It should be pointed out that for the wider range of parameters, say larger computation region or smaller α, scheme 1 may often fail to work, while scheme 2 can still work well due to its good numerical stability which might result from the influence of nonlinear diffusion could be suppressed by using Eq. (21) to adjust relaxation times. What makes the difference between schemes 1 and 2 needs to be studied further.

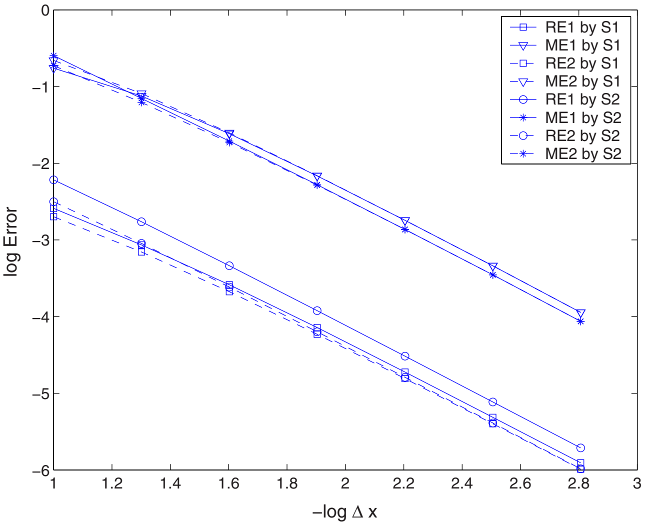

FIG. 6. (Color online) Accuracy test for the two schemes at $t=1$ for $\delta=1.2$ and $a=0.01$. $S1$: scheme 1; $S2$: scheme 2.

Example 4.5. We consider the two-dimensional SGE [44]

$$u_{tt}=u_{xx}+u_{yy}-\sin(u), \tag{35}$$

in the spacial region $\Omega=\{(x,y)|-a<x<a,-b<y<b\}$. The boundary conditions associated with Eq. (35) impose a zero gradient along the boundary Γ of Ω,

$$u_x=0,\quad x=\pm a;\quad u_y=0,\quad y=\pm b, \tag{36}$$

while the initial conditions are given by

$$u(x,y,0)=f(x,y),\quad u_t(x,y,0)=g(x,y). \tag{37}$$

Note that Eq. (35) is different from the DE with a source term since it contains u_{tt}. Using the idea in Ref. [38], Eq. (3) can be taken as

$$\begin{aligned} f_j^{\mathrm{eq}}(\mathbf{x},t) &= \omega_j\left[u_t+\frac{c_s^2(u-u_t)\mathbf{I}:(\mathbf{c}_j\mathbf{c}_j-c_s^2\mathbf{I})}{2c_s^4}\right] \\ &= \omega_j\left[u_t+\frac{(u-u_t)(\mathbf{c}_j^2-2c_s^2)}{2c_s^2}\right], \end{aligned} \tag{38}$$

such that

$$\sum_j f_j=\sum_j f_j^{\mathrm{eq}}=u_t,\quad \sum_j \mathbf{c}_j f_j^{\mathrm{eq}}=\mathbf{0},\quad \sum_j \mathbf{c}_j\mathbf{c}_j f_j^{\mathrm{eq}}=c_s^2u\mathbf{I} \tag{39}$$

with $c_s^2(\tau-\frac{1}{2})\Delta t=1$. We use the difference scheme to compute u_t: $u(\mathbf{x},t+\Delta t)=\Delta t\Sigma_j f_j(\mathbf{x},t+\Delta t)+u(\mathbf{x},t)$.

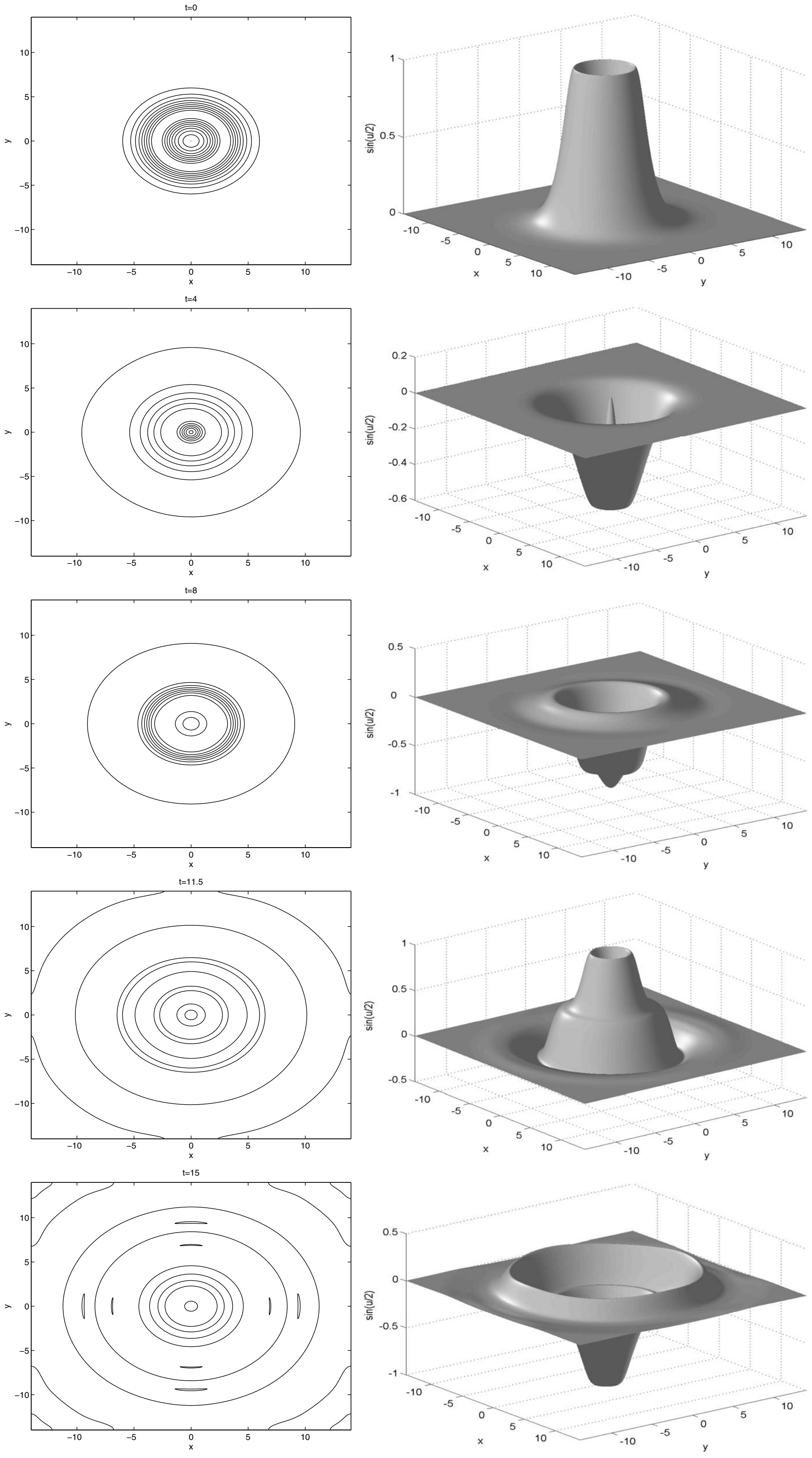

FIG. 7. Collision of one ring solitons: the function $\sin(u/2)$ (from top to bottom: $t=0$, 4, 8, 11.5, and 15).

In simulations, three cases are considered and the wave parameters are taken as $\alpha=4$, $\beta=4.13$ and $\gamma=1/0.436$ as in Ref. [44] for comparison. The grid and time steps are set to be $\Delta x=0.05$ and $\Delta t=0.001$, respectively, for all cases.

For the particular case of circular ring solitons, we choose

$$f(x,y) = \alpha \arctan \exp\{3 - \sqrt{x^2+y^2}\}, \quad g(x,y) = 0, \quad (40)$$

over the 2D domain $-14 \leqslant x$, $y \leqslant 14$, which was also used in Ref. [44]. The simulation results via the LBGK model at

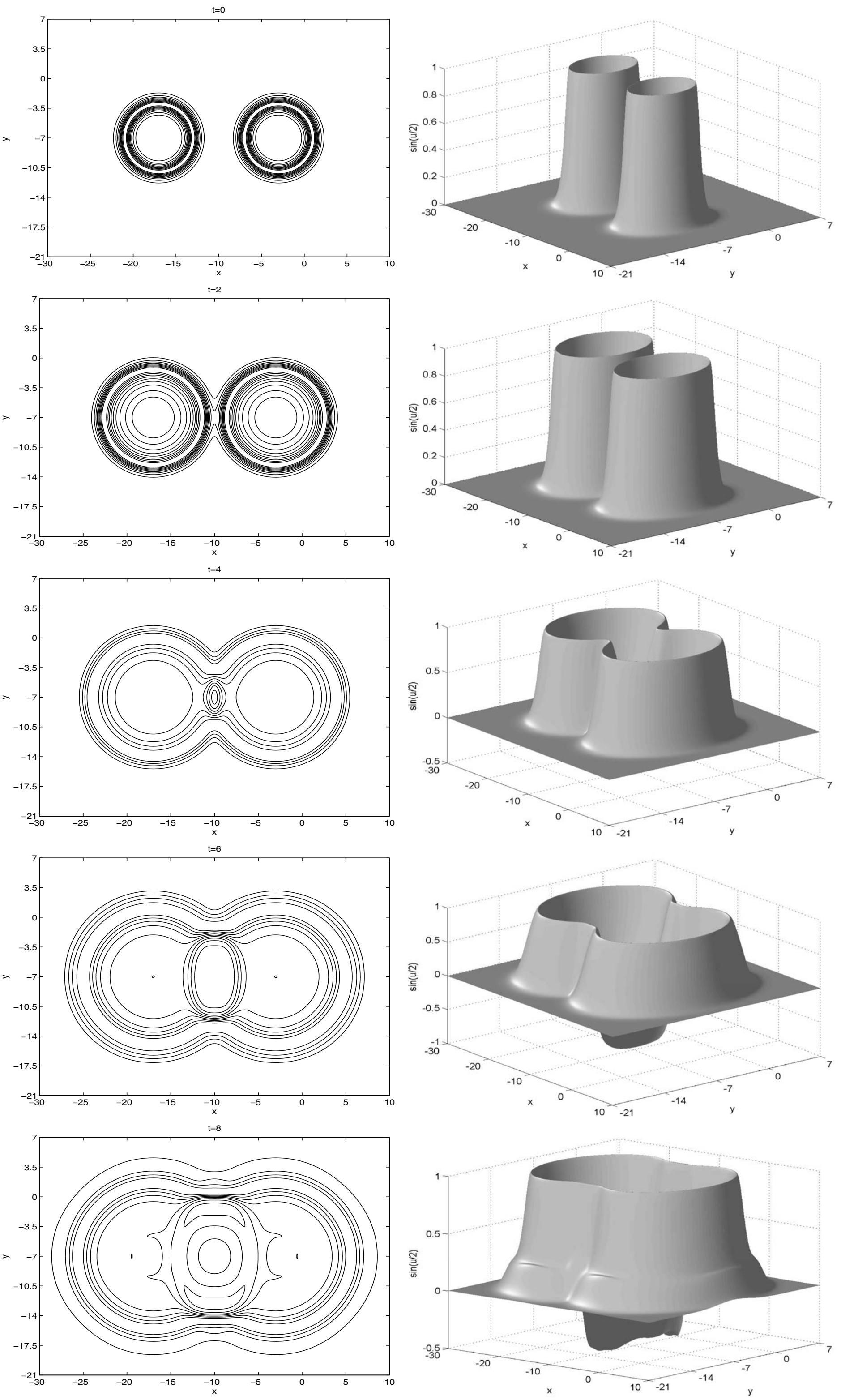

FIG. 8. Collision of two ring solitons: the function $\sin(u/2)$ (from top to bottom: $t=0$, 2, 4, 6, and 8).

$t=0$, 4, 8, 11.5, and 15 are given in terms of $\sin(u/2)$ in Fig. 7.

Further, when collisions of two circular solitons are considered, we choose the following standard settings [44]:

$$f(x,y)=\alpha\sum_{j=1}^{2}\ \arctan\exp\{\gamma[4-\sqrt{(x+x_j)^2+(y+y_j)^2}]\},$$

$$g(x,y)=\beta\sum_{j=1}^{2}\ \operatorname{sech}\{\gamma[4-\sqrt{(x+x_j)^2+(y+y_j)^2}]\},\quad (41)$$

where $-30\leqslant x\leqslant 10$, $-21\leqslant y\leqslant 7$, $\{(x_j,y_j)\}=\{(3,7),(17,7)\}$. Numerical simulations are presented in Fig. 8 in terms of $\sin(u/2)$ at $t=0$, 2, 4, 6, and 8, respectively.

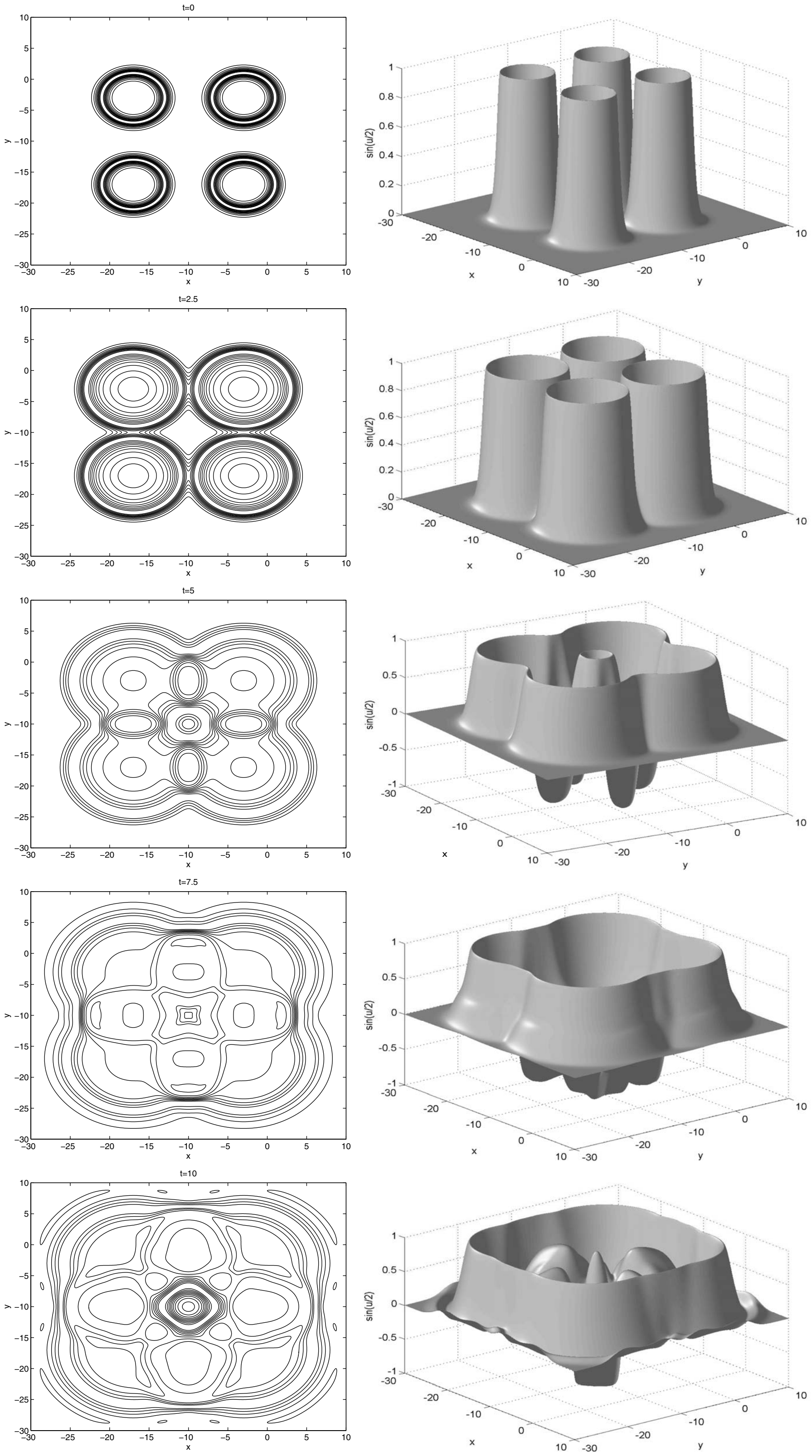

FIG. 9. Collision of four ring solitons: the function $\sin(u/2)$ (from top to bottom: $t=0$, 2.5, 5, 7.5, and 10).

Finally, for collisions of four circular solitons, as in Ref. [44] we take that

$$f(x,y) = \alpha \sum_{j=1}^{4} \arctan \exp\{\gamma[4 - \sqrt{(x+x_j)^2 + (y+y_j)^2}]\},$$

$$g(x,y) = \beta \sum_{j=1}^{4} \operatorname{sech}\{\gamma[4 - \sqrt{(x+x_j)^2 + (y+y_j)^2}]\}, \quad (42)$$

where $-30 \leqslant x, \quad y \leqslant 10$, $\{(x_j, y_j)\} = \{(3,3),(3,17),(17,3),(17,17)\}$. Numerical simulations are plotted in Fig. 9 in terms of $\sin(u/2)$ at $t=0$, 2.5, 5, 7.5, and 10, respectively.

From Figs. 7–9 it can be found that the numerical results here are in excellent agreement with those in Ref. [44].

V. CONCLUSION

In the present work, we have developed a unified LBGK model for nD nonlinear convection and isotropic-diffusion equation, and two LBGK schemes are derived from the model for the NCDE with a nonlinear diffusion term. Unlike traditional numerical methods which solve for macroscopic variables, the model has the advantages of standard LBGK model, which are borrowed from kinetic theory, such as linearity of the convection operator in velocity space, simplicity and symmetry of scheme, ease in coding and intrinsical parallelism [3]. Detailed numerical tests of the proposed model and that using standard LBGK evolution equation are carried out for different types of convection-diffusion-like equations, including the 1D nonlinear Schrödinger equation, 2D complex Ginzburg-Landau equation, 2D Burgers-Fisher equation, 2D NHCE, and 2D sine-Gordon equation. It is found that the simulation results agree well with the analytical and numerical solutions reported in previous studies, which shows that the LBM has potentials in simulating NCDE. It is also found that the stability of scheme 2 for NHCE is better than that of scheme 1, while the accuracy of scheme 2 is a little lower than that of scheme 1. Unlike scheme 1 in which a fixed relaxation time is used, the relaxation time in scheme 2 varies with position $\mathbf{x}$ and time t according to Eq. (21), thus the influence of nonlinear diffusion might be suppressed by using adjustable relaxation times. What makes the difference between schemes 1 and 2 needs to be studied further. As pointed out in Refs. [37,38], in order to attain better accuracy the LB model for complex equations requires a relatively small time step Δt and the proper range is from 10^{-4} to 10^{-5}.

The idea of the proposed model can be directly applied to derive the complex-valued versions of other existing LB models for nonlinear evolutionary equations by utilizing complex-valued distribution functions and a relaxation time, and may be used to derive the corresponding LB model for NCDE with anisotropic diffusivity. Nevertheless, some important issues, such as how to improve the accuracy, efficiency and stability of complex-valued LB models or the LB models for highly nonlinear evolutionary equations need further studies.

ACKNOWLEDGMENTS

The authors are grateful to referees for their valuable comments and suggestions. This work was supported by the National Science Foundation of China (Grant Nos. 60773195 and 50606012).

[1] R. Benzi, S. Succi, and M. Vergassola, Phys. Rep. **222**, 145 (1992).
[2] Y. H. Qian, S. Succi, and S. A. Orszag, Annu. Rev. Comput. Phys. **3**, 195 (1995).
[3] S. Chen and G. D. Doolen, Annu. Rev. Fluid Mech. **30**, 329 (1998).
[4] B. C. Shi, Z. L. Guo, and N. C. Wang, Chin. Phys. Lett. **19**, 515 (2002).
[5] R. G. M. van der Sman, Phys. Rev. E **74**, 026705 (2006).
[6] Z. L. Guo, C. G. Zheng, B. C. Shi, and T. S. Zhao, Phys. Rev. E **75**, 036704 (2007).
[7] C. H. Sun, Phys. Rev. E **58**, 7283 (1998).
[8] Z. L. Guo and T. S. Zhao, Phys. Rev. E **66**, 036304 (2002).
[9] Y. S. Xu, Y. J. Zhong, and G. X. Huang, Chin. Phys. Lett. **21**, 1298 (2004).
[10] H. P. Fang and S. Y. Chen, Chin. Phys. **13**, 47 (2004).
[11] A. J. C. Ladd and R. Verberg, J. Stat. Phys. **104**, 1191 (2001).
[12] X. He, X. Shan, and G. D. Doolen, Phys. Rev. E **57**, R13 (1998).
[13] L.-S. Luo and S. S. Girimaji, Phys. Rev. E **67**, 036302 (2003).
[14] S. Ponce Dawson, S. Y. Chen, and G. D. Doolen, J. Chem. Phys. **98**, 1514 (1993).
[15] R. Blaak and P. M. Sloot, Comput. Phys. Commun. **129**, 256 (2000).
[16] X. M. Yu and B. C. Shi, Appl. Math. Comput. **181**, 958 (2006).
[17] M. R. Swift, E. Orlandini, W. R. Osborn, and J. M. Yeomans, Phys. Rev. E **54**, 5041 (1996).
[18] Z. L. Guo, B. C. Shi, and N. C. Wang, J. Sci. Comput. **14**, 291 (1999).
[19] X. Y. He, N. Li, and B. Goldstein, Mol. Simul. **25**, 145 (2000).
[20] R. G. M. van der Sman and M. H. Ernst, J. Comput. Phys. **160**, 766 (2000).
[21] B. C. Shi, B. Deng, R. Du, and X. W. Chen, Comput. Math. Appl. **55**, 1568 (2008).
[22] X. M. Yu and C. Shi, Chin. Phys. B **15**, 1441 (2006).
[23] G. W. Yan, J. Comput. Phys. **161**, 61 (2000).
[24] X. X. Zhang *et al.*, Adv. Water Resour. **25**, 1 (2002).
[25] I. Rasin, S. Succi, and W. Miller, J. Comput. Phys. **206**, 453 (2005).
[26] I. Ginzburg, Adv. Water Resour. **28**, 1171 (2005).
[27] D. A. Meyer, J. Stat. Phys. **85**, 551 (1996).
[28] S. Succi and R. Benzi, Physica D **69**, 327 (1993).
[29] S. Succi, Phys. Rev. E **53**, 1969 (1996).
[30] B. Boghosian and W. Taylor IV, Int. J. Mod. Phys. C **8**, 705 (1997).
[31] J. Yepez and B. Boghosian, Comput. Phys. Commun. **146**, 280 (2002).
[32] J. Yepez, J. Stat. Phys. **107**, 203 (2002).
[33] G. Vahala, J. Yepez, and L. Vahala, Phys. Lett. A **310**, 187 (2003).
[34] G. Vahala, L. Vahala, and J. Yepez, Physica A **362**, 215 (2006).
[35] S. Palpacelli and S. Succi, Phys. Rev. E **75**, 066704 (2007).
[36] S. Palpacelli and S. Succi, Phys. Rev. E **77**, 066708 (2008).
[37] L. H. Zhong, S. D. Feng, P. Dong, and S. T. Gao, Phys. Rev. E **74**, 036704 (2006).
[38] B. C. Shi, Lect. Notes Comput. Sci. **4487**, 818 (2007).

[39] Z. L. Guo, C. G. Zheng, and B. C. Shi, Phys. Rev. E **65**, 046308 (2002).

[40] Z. L. Guo, C. G. Zheng, and B. C. Shi, Chin. Phys. **11**, 366 (2002).

[41] Y. Xu and C.-W. Shu, J. Comput. Phys. **205**, 72 (2005).

[42] C. T. Zhou, M. Y. Yu, and X. T. He, Phys. Rev. E **73**, 026209 (2006).

[43] A.-M. Wazwaz, Appl. Math. Comput. **169**, 321 (2005).

[44] Q. Sheng, A. Q. M. Khaliq, and D. A. Voss, Math. Comput. Simul. **68**, 355 (2005).